ACS OMEGA

http://pubs.acs.org/journal/acsodf

Article

Preparation of Nitrogen-Doped Cellulose-Based Porous Carbon and Its Carbon Dioxide Adsorption Properties

Yifan Tan, Xiaoqiang Wang, Shen Song, Meijiao Sun, Yuhua Xue, and Guangzhi Yang*

Cite This: *ACS Omega* 2021, 6, 24814–24825

Read Online

ACCESS | Metrics & More | Article Recommendations

ABSTRACT: Nitrogen-doped cellulose-based porous carbon materials were obtained by hydrothermal method and KOH chemical activation together with melamine as a nitrogen-doping precursor. The effects of hydrothermal temperature on the microstructure and surface morphology of the products were mainly studied. Also, the carbon dioxide adsorption capacity of the prepared porous carbon was investigated. It was found that when the hydrothermal carbonization temperature was 270 °C and the mass ratio of cellulose and melamine was 1:1, the largest micropore specific surface area of 1703 $m^2 \cdot g^{-1}$ and micropore volume of 0.65 $cm^3 \cdot g^{-1}$ were obtained, with a nitrogen-doping composition of 1.68 atom %. At the temperature of 25 °C and under the pressure of 0.1, 0.2, 0.3, and 0.4 MPa, the adsorption amount of CO_2 was 1.56, 3.79, 5.42, and 7.34 $mmol \cdot g^{-1}$, respectively. Also, the adsorption process of CO_2 was in good accordance with the Freundlich isotherm model.

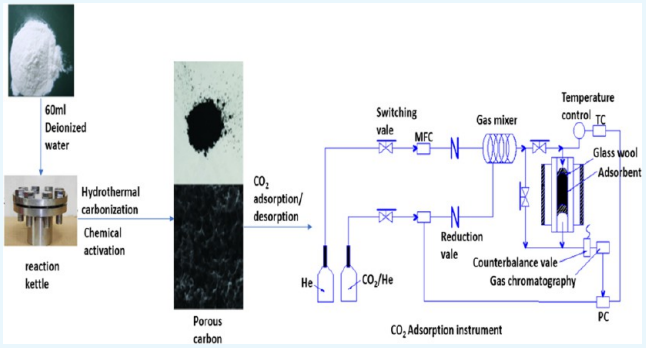

1. INTRODUCTION

Greenhouse effect has become a global environmental problem, and CO_2 is a significant greenhouse gas affecting climate change.[1] The use of fossil fuels has led to a rapid increase in the amount of CO_2 in the atmosphere.[2] Excessive emissions of CO_2 have caused a series of environmental issues, including global warming, rising sea levels, and ocean acidification, which hinder the survival and development of human society.[3] Therefore, decreasing the emission of CO_2 and controlling the amount of CO_2 in the atmosphere are urgently required to relieve the pressure of global warming.

CO_2 capture and storage (CCS) is a technology that uses currently available means to separate carbon dioxide from a designated source, transport it by a pipeline or ship to a designated location, and then store it underground or in an ocean.[4] In general, CCS consists of three steps:[5] (1) CO_2 emissions from burning fossil fuels are separated and purified before entering the atmosphere. (2) The captured CO_2 is transformed to a liquid state under high pressure and transported to a storage site. (3) The liquid CO_2 is injected directly into the 800 m deep rock.

Recently, many methods are used for CCS, such as solvent absorption,[6] cryogenics,[7] membrane separation,[8] solid absorbent,[9] etc. Solid adsorption technology has been widely applied due to its low energy consumption, good stability, simple process, small equipment loss, and other characteristics. Generally, commonly used solid adsorbents include zeolite,[10] mesoporous silica,[11] metal−organic frameworks (MOFs),[12] porous polymer materials,[13] porous carbon,[14] etc. These materials exhibit satisfactory properties, but their industrial applications are limited due to their relatively high cost of synthesis and application. Therefore, it is necessary to investigate and explore low-cost, high-capacity, and environmentally safe CO_2 capturing materials.[15] Among them, porous carbon materials have the advantages of lightweight, large specific surface area, good chemical and thermal stability, low price, and so on, and they have great application potential.[16]

An outstanding advantage of porous carbons is their easy synthesis by almost any raw material containing a certain amount of carbon such as coal,[17] petroleum coke,[18] polymers,[19,37] and biomass materials.[20−26] Nowadays, many methods are used to prepare porous carbon materials such as template,[27] hydrothermal carbonization,[28] and activation.[29] Porous carbon materials prepared by hydrothermal carbonization method have the advantages of convenient operation, high carbon yield, and low cost, which is a sustainable way to produce carbon. Nowadays, biomass materials are widely used as precursors for the preparation of porous carbon materials,

Received: July 12, 2021
Published: September 15, 2021

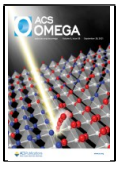

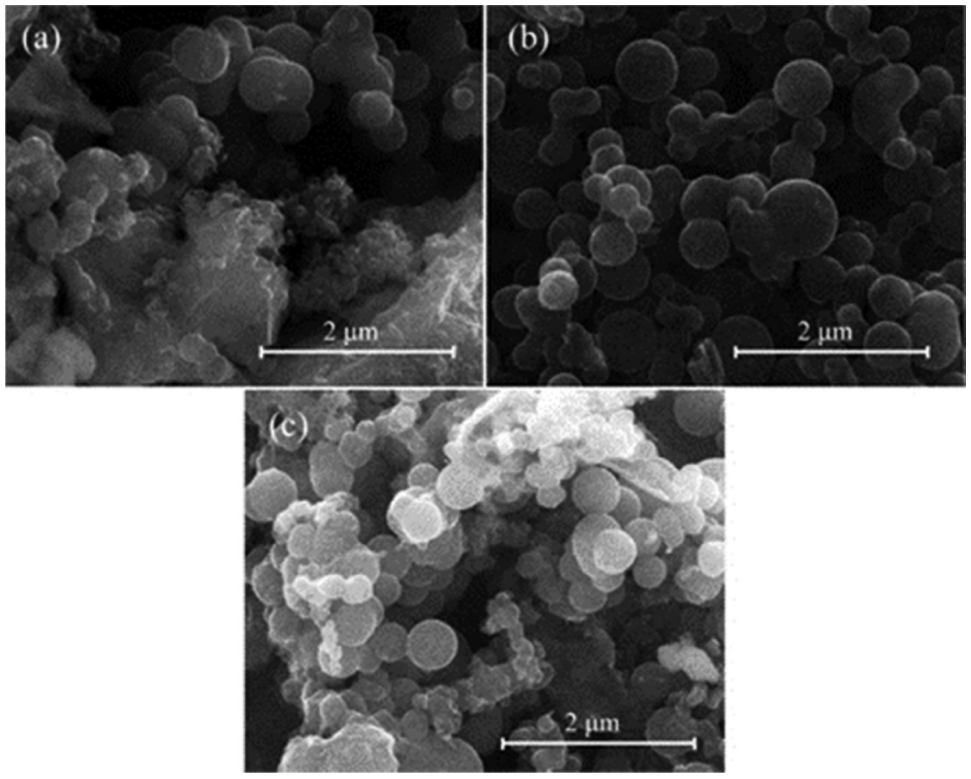

Figure 1. SEM images of (a) NCe-240-1, (b) NCe-270-1, and (c) NCe-300-1.

including wheat straw,[20] sawdust,[21] palm seed,[22] corn stalk,[23] cellulose,[24] glucose,[25] and so on. Among these precursors, cellulose is an ideal model component of biomass because of its wide source and low price. The surface chemical properties of porous carbon have a strong effect on its adsorption capacity.[26] Also, because CO_2 is an acid gas, introducing basic groups (e.g., basic nitrogen functionalities) on the surface of porous carbon can increase its ability to adsorb CO_2.[30,31]

The synthesis of nitrogen-doped porous carbons has been achieved by mainly two methods: (1) carbonization of N-containing precursors[32] and (2) co-carbonization of mixtures of N-containing organic compounds with N-free materials;[33] the second method involves (1) heat treatment of porous carbons with N-containing gases[34] or N-containing organic compounds[35] and (2) impregnation with amine functional groups.[36] Nowadays, many new nitrogen-doped porous carbon materials with controlled pore structure and excellent CO_2 adsorption capacity have been synthesized by different preparation methods. Park et al.[13] prepared a series of alkali-activated porous carbons (TOKs) by a single-pot polymerization−carbonization−activation method using KOH as a dynamic molecular porogen. The fabricated materials possess a tunable porous network with a high specific surface area (up to 2847 m^2/g), large micropore volume (1.369 cm^3/g), and a large population of micropores in the sub-nanometer range. At 1 bar and 25 °C, activated carbons TOK-800 and TOK-900 adsorbed 6.57 mmol/g of CO_2 and 6.85 mmol/g of CO_2. Hu et al.[38] prepared porous carbon materials from the waste biomass lotus leaf by carbonization, melamine post-treatment, and KOH activation. These materials show good CO_2 adsorption abilities, up to 3.87 and 5.89 mmol/g at 25 and 0 °C under 1 bar, respectively. Also, Hu et al.[39] prepared N-doped porous carbons from commercial phenolic resin, urea, and KOH by the conventional carbonization−nitridation−activation three-step method. The adsorbents show superior CO_2 uptake of 5.01 and 7.47 mmol/g at 25 °C and 0 °C under 1 bar, respectively. Pang et al.[40] prepared porous carbon materials from hazelnut shells by the nitrogen-doping technology with KOH activation. The prepared porous carbons show a highly developed porous structure and a high N content, whereas the prepared porous carbon materials have a high CO_2 adsorption capacity of 6.34 mmol/g at 1 bar. Herein, considering all of the beneficial attributes and low price of an adsorbent, these new research studies reported a facile synthesis of a series of fine powdered ACs from an inexhaustible biopolymer "cellulose." Park et al.[25] prepared heteroatom-doped (N, S) porous carbons by solvent-free one-pot carbonization and in situ activation of cellulose in the presence of urea/thiourea and KOH. The adsorbents exhibit a significantly large micropore volume (0.7135 cm^3/g), an abundance of narrow micropores (<0.94 nm), and an optimum pyrrolic nitrogen content (58%), which leads to efficient CO_2 adsorption (6.72 mmol/g at 0 °C and 4.38 mmol/g at 25 °C/1 bar). Kamran et al.[41] prepared porous carbon materials from cellulose by hydrothermal carbonization technology and nitrogen-doping technology with KOH activation. The prepared porous carbons show a high CO_2 adsorption capacity of 6.75 mmol/g at 1 bar. Therefore, the present work clearly demonstrates that nitrogen-enriched surfaces can enhance the CO_2 adsorption properties. Moreover, nitrogen-doped porous carbon is considered a promising adsorbent and has received a lot of attention in the last decade. There is still a lack of analysis and research on the preparation of porous carbon materials with cellulose and melamine as raw materials and their CO_2 adsorption properties.

In this paper, different porous carbon samples were prepared from cellulose and melamine by changing the hydrothermal carbonization temperature and the ratio of melamine. The surface morphology, elemental composition, and pore structure

https://doi.org/10.1021/acsomega.1c03664
ACS Omega 2021, 6, 24814−24825

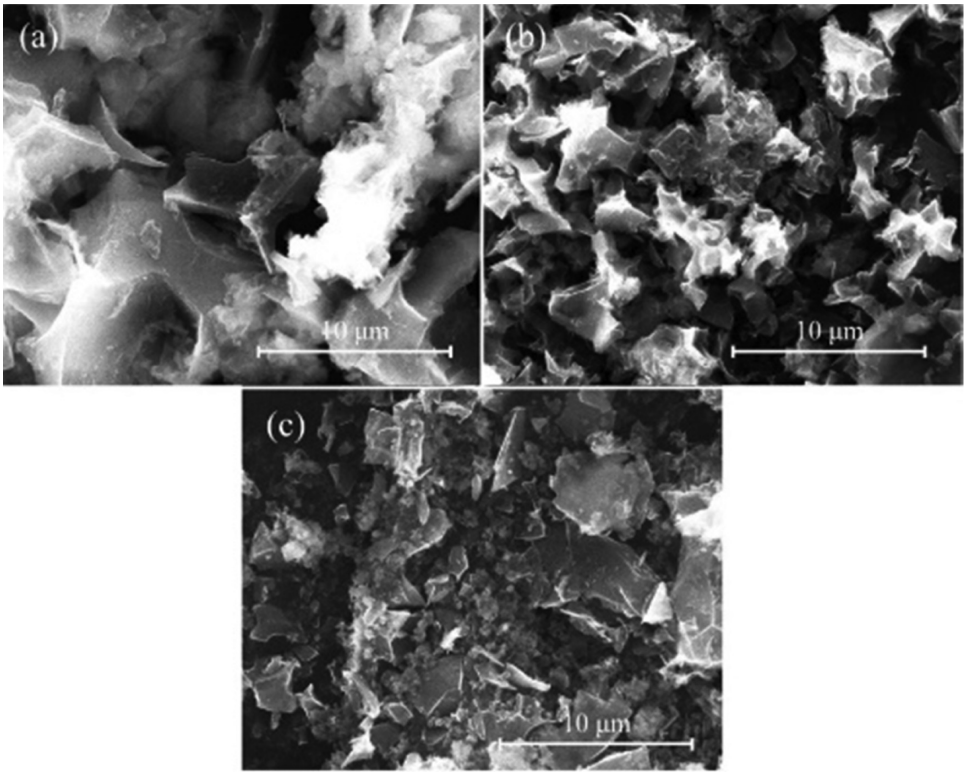

Figure 2. SEM images of (a) ANCe-240-1, (b) ANCe-270-1, and (c) ANCe-300-1.

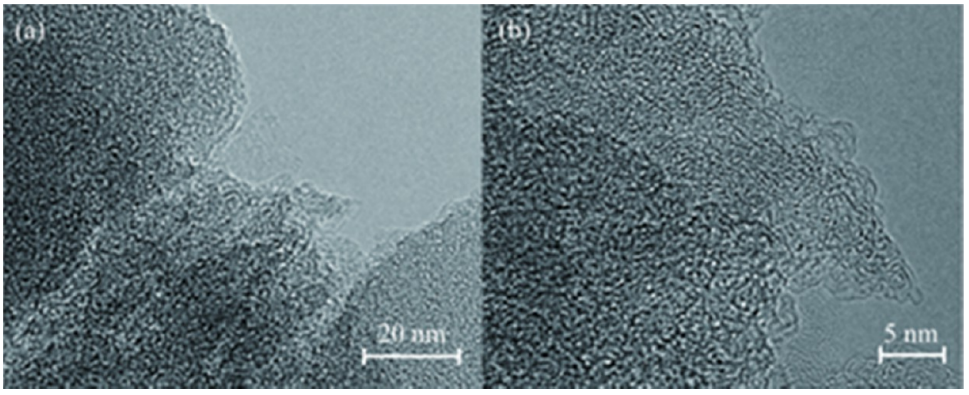

Figure 3. TEM images of ANCe-270-1: (a) low magnification and (b) high magnification.

of the porous carbon samples at different hydrothermal temperatures and melamine ratios were compared. Also, the CO_2 adsorption properties of the carbon materials at the pressure of 0.1−0.4 MPa were investigated. At the same time, the dynamic adsorption mechanism was studied and the corresponding adsorption mechanism was proposed.

2. RESULTS AND DISCUSSION

2.1. Effect of Hydrothermal Temperature. Nitrogen-doped hydrothermal products were prepared from cellulose and melamine with a mass ratio of 1:1 at 240, 270, and 300 °C, respectively. Scanning electron microscopy (SEM) images of the nitrogen-doped hydrothermal products are shown in Figure 1. It can be seen in Figure 1a that the product is at a hydrothermal reaction temperature of 240 °C. Because cellulose was initially hydrolyzed to produce cellobiose, glucose, and other substances, the reaction degree with melamine and carbonization was low, leading to less spherical morphology

Table 1. Elemental Composition of Different Samples

sample	C (atom %)	N (atom %)	O (atom %)	N/C (at/at)	O/C (at/at)
NCe-240-1	56.12	31.20	12.68	0.56	0.23
NCe-270-1	58.50	31.92	9.58	0.55	0.16
NCe-300-1	58.69	31.94	9.37	0.54	0.15
ANCe-240-1	88.33	0.93	10.74	0.01	0.12
ANCe-270-1	90.82	1.68	7.50	0.02	0.08
ANCe-300-1	91.05	1.57	7.38	0.02	0.08

transformation. Figure 1b,c shows the nitrogen-doped hydrothermal products prepared at higher temperatures (270 and 300 °C, respectively). Due to the complete hydrolysis of cellulose, hydrolysate and melamine in the hydrothermal environment experienced a series of dehydration, condensation, polymerization, and aromatization reactions; hydrothermal products were mostly transformed into spherical particles.

https://doi.org/10.1021/acsomega.1c03664
ACS Omega 2021, 6, 24814−24825

Table 2. Hydrothermal Temperature Effect on the Yields of Different Periods

sample	yield (wt %)		
	hydrothermal carbonization	KOH activation	total
ANCe-240-1	65.46	25.60	16.76
ANCe-270-1	59.32	28.91	17.15
ANCe-300-1	55.17	30.75	16.96
ACe-240	61.29	33.89	20.77
ACe-270	54.93	36.72	20.17
ACe-300	52.47	37.56	19.71

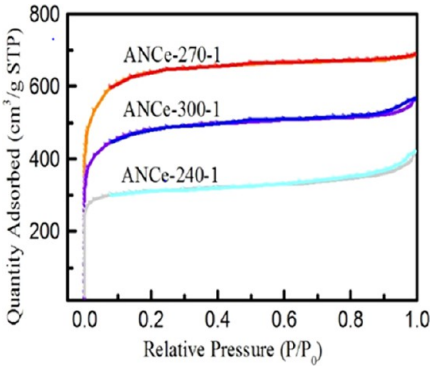

Figure 4. N_2 adsorption and desorption isotherms of different samples.

The nitrogen-doped porous carbon materials were prepared by further KOH activation and carbonization. SEM images of the materials after activation are shown in Figure 2. It can be seen in Figure 2a that the surface morphology of the carbonized product changes from spherical to irregular smooth block surface morphology. This was attributed to the metallic potassium vapor generated by the reaction between carbon materials and KOH in the process of high-temperature carbonization, which led to the change of morphology and played a promoting role in the activation of carbon materials.[41] Figure 2b,c shows that the fragmented particles of carbonized porous carbon at high temperatures (270, 300 °C) are small. At high temperatures, the degree of carbonization was high and the surface formed many chemical active sites, which were conducive to the formation of pores and KOH activation. Transmission electron microscopy (TEM) images of ANCe-270-1 are shown in Figure 3a,b, in which many irregular micropores can be observed.

Elemental analysis of nitrogen-doped porous carbon by energy-dispersive X-ray spectroscopy (EDS) is shown in Table 1. It can be seen that with the increase in the reaction temperature, the contents of C and N in the hydrothermal samples increase, while the contents of O decrease. In the samples, after activation and carbonization (ANCe-240-1, ANCe-270-1, ANCe-300-1), the content of the N element

Table 3. Different Pore Structure Parameters of Samples

sample	S_{BET} [a] ($m^2 \cdot g^{-1}$)	V_{total} [b] ($cm^3 \cdot g^{-1}$)	S_{micro} [c] ($m^2 \cdot g^{-1}$)	V_{micro} [c] ($cm^3 \cdot g^{-1}$)	D_p [d] (nm)
ANCe-240-1	1043	0.68	759	0.46	2.48
ANCe-270-1	1703	1.06	1203	0.65	2.21
ANCe-300-1	1378	0.95	1046	0.58	2.37
ACe-240	934	0.61	454	0.36	2.62
ACe-270	1259	0.97	964	0.51	2.39
ACe-300	1151	0.86	735	0.51	2.43

[a]BET surface area. [b]Total pore volume measure at P/P_0 = 0.99. [c]Micropore surface area and micropore volume estimated d < 2 nm by the DFT method. [d]Average pore diameter.

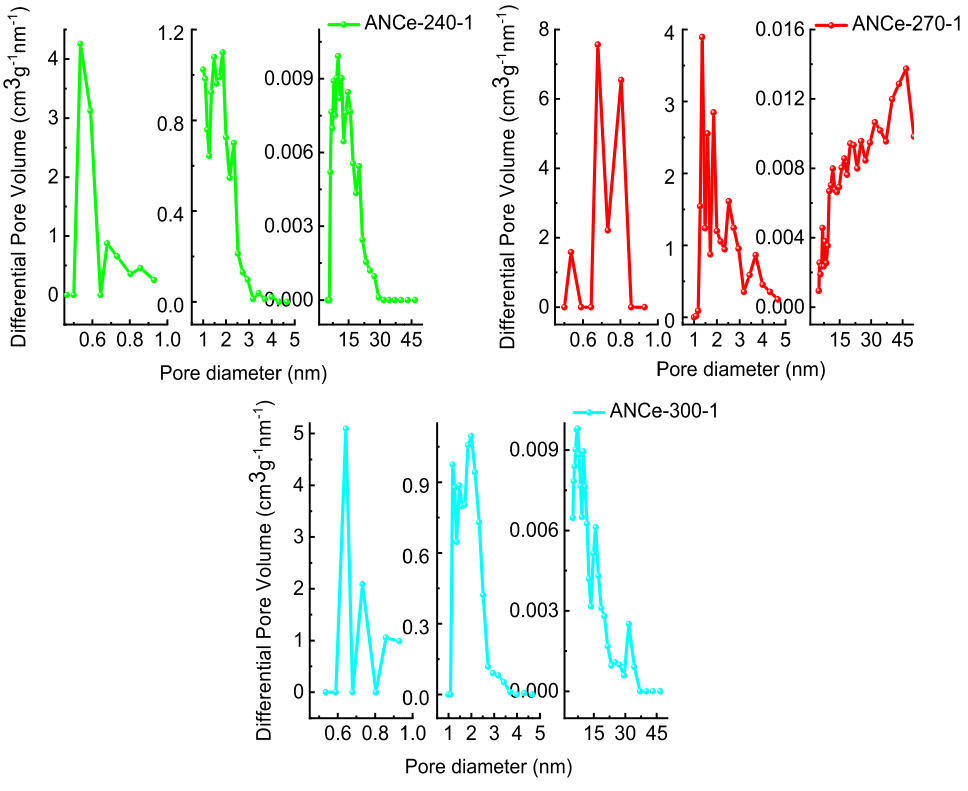

Figure 5. Pore size distribution of different samples.

https://doi.org/10.1021/acsomega.1c03664
ACS Omega 2021, 6, 24814−24825

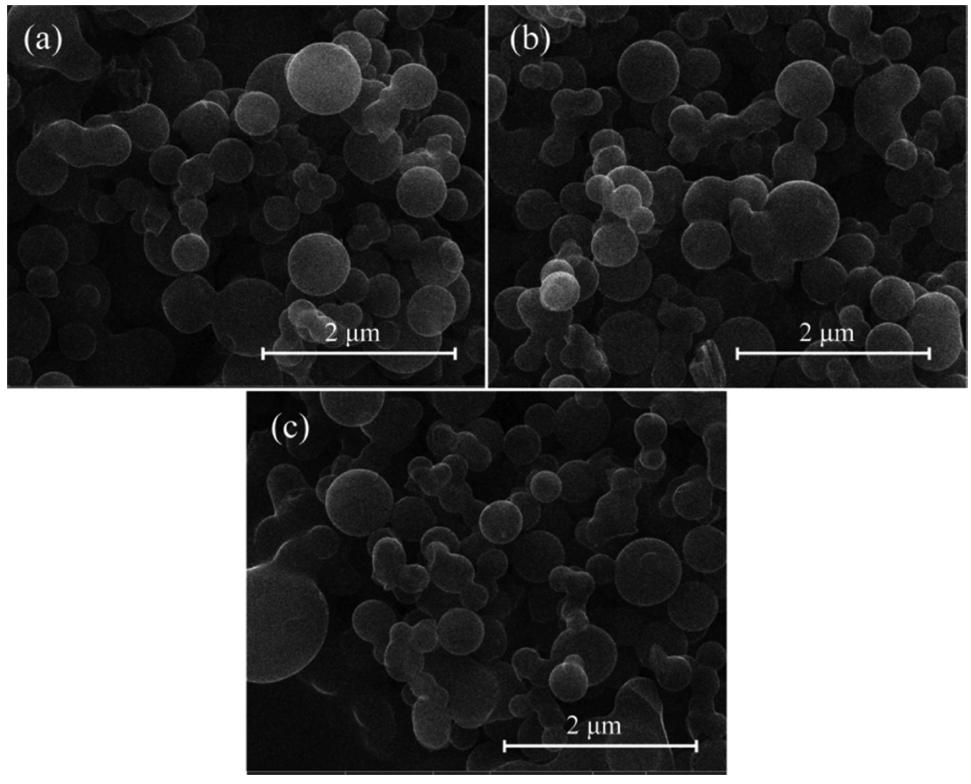

Figure 6. SEM images of hydrothermal products: (a) NCe-270-0.5, (b) NCe-270-1, and (c) NCe-270-3.

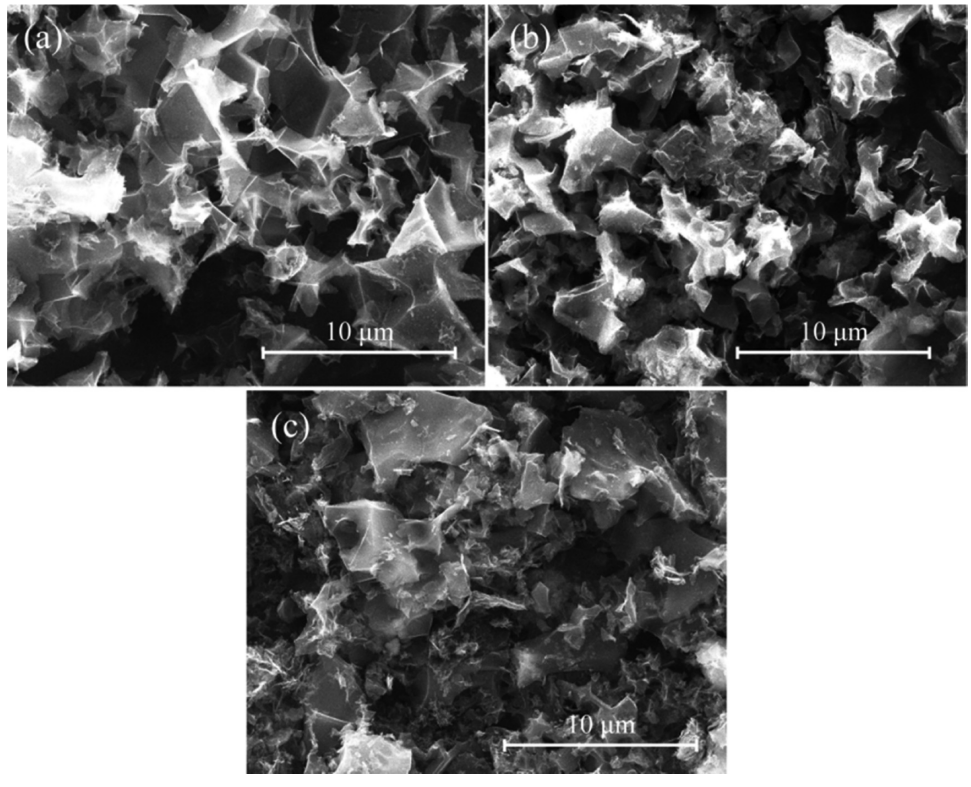

Figure 7. SEM images of porous carbon: (a) ANCe-270-0.5, (b) ANCe-270-1, and (c) ANce-270-3.

decreased obviously, while the content of O decreased slightly. In the process of activation, some small molecules of N and O were generated, which destroyed the spherical morphology and facilitated the formation of pores. The loss of N element in the activated porous carbon sample was great. This indicated that some unstable N-containing groups reacted violently with KOH or decomposed in the activation.[42] The sample of ANCe-270-1 had the highest nitrogen content of 1.68 atom %.

Table 2 lists the yield of different samples during hydrothermal and activated carbonization, respectively. Because

https://doi.org/10.1021/acsomega.1c03664
ACS Omega 2021, 6, 24814−24825

Table 4. Elemental Composition of Different Nitrogen-Doped Samples

sample	C (atom %)	N (atom %)	O (atom %)	N/C (at/at)	O/C (at/at)
NCe-270-3	70.08	15.66	14.26	0.22	0.20
NCe-270-1	58.50	31.92	9.58	0.55	0.16
NCe-270-0.5	50.95	42.46	6.59	0.83	0.13
ANCe-270-3	90.66	0.69	8.65	0.01	0.10
ANCe-270-1	90.82	1.68	7.50	0.02	0.08
ANCe-270-0.5	88.33	1.75	7.12	0.02	0.08

Table 5. Yields of Samples Prepared at Different Melamine Ratios

	yield (wt %)		
sample	hydrothermal carbonization	KOH activation	total
ANCe-270-3	56.27	32.47	18.27
ANCe-270-1	59.32	28.91	17.15
ANCe-270-0.5	66.21	23.46	15.53

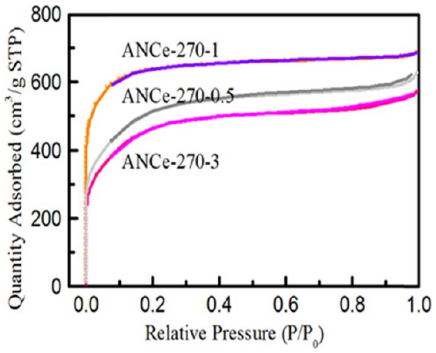

Figure 8. N_2 adsorption and desorption isotherms of different samples.

melamine decomposes more easily after heating compared with cellulose, which has a higher carbonization residue, the mixture of melamine and cellulose has a lower carbonization yield compared with cellulose alone.[43] On the other hand, the activation yields of all of the melamine and cellulose mixtures products are higher than the half yields of all products based on cellulose alone, indicating that melamine is not completely decomposed and partially doped into the cellulose transferred carbons. The total yield of the nitrogen-doped samples is about 17%.

The N_2 adsorption−desorption of porous carbons was performed for further studying the pore structure of the materials. According to the classification of adsorption isotherms by IUPAC, Figure 4 shows that the isotherms of nitrogen-doped samples with different hydrothermal temperatures are all typical I isotherms. The results show that all of the samples have abundant micropores. In the range of low relative pressure ($P/P_0 < 0.1$), with the increase of pressure, the N_2 adsorption capacity of the sample increases, indicating that the process was mainly micropore filling. With the increase in relative pressure, the N_2 adsorption capacity tends to be stable, indicating multilayer adsorption of the adsorbent. Figure 5 shows the pore size distribution of different nitrogen-doped porous carbon samples. The Brunauer−Emmett−Teller (BET) surface area, pore volume, and average pore size of the prepared samples are listed in Table 3. It shows the nitrogen-doped samples have a large specific surface area and large pore volume. The main reason is that in the chemical activation process, small gas molecules containing N groups escape from the surface, which is beneficial to the formation of pores. ANCe-270-1 has the largest specific surface area (1703 $m^2\ g^{-1}$) and pore volume (1.06 $cm^3\ g^{-1}$).

2.2. Effect of Melamine Ratio. Cellulose and melamine are mixed at different mass ratios, and the SEM images of hydrothermal products at 270 °C are shown in Figure 6. It shows that the ratio of cellulose and melamine has little effect on the morphology of hydrothermal products at the same hydrothermal temperature.

Figure 7 shows the SEM images of nitrogen-doped porous carbon materials prepared after KOH activation. It can be seen that the original spherical morphology turned into small powders. The possible reason was that KOH reacted violently with C and N in the process of high-temperature carbonization, which resulted in K vapor and other small molecule gases escaping from the surface and destroyed the morphology of the samples.[44]

The elemental analysis of the nitrogen-doped porous carbon by EDS is shown in Table 4. It can be seen that with the increase in melamine ratio, the content of N in hydrothermal products gradually increased and the value of N/C gradually increased. In the process of activation, the content of N decreased rapidly. In particular, the nitrogen content of the sample ANCe-270-0.5 decreased from 42.46 to 1.75 atom %, indicating that the nitrogenous groups generated by the hydrothermal process were unstable and decreased rapidly in the chemical activation process. This conclusion is in good accordance with Table 1.

Table 5 shows the yields of the samples prepared at different melamine ratios. It can be seen that with the increase in melamine, the yield of hydrothermal carbonization gradually increased, the yield of KOH activation decreased, and the total yield showed a downward trend. As discussed above, the addition of melamine leads to a decrease in activation yield, so the higher the ratio of melamine, the lower is the yield.

Figure 8 shows the N_2 adsorption and desorption isotherms of the samples at 77 K. Their pore size distributions are shown in Figure 9. Their pore structure parameters are shown in Table 6. According to the classification of adsorption isotherms by IUPAC, the isotherms of nitrogen-doped samples were typical I isotherms. It is indicated that the nitrogen-doped porous carbon samples had abundant micropores. By comparing the data of pore size distribution and pore size, it could be seen that with the increase in melamine, the specific surface area and pore volume of micropores first increased and then decreased. The formation of micropores are promoted when the nitrogen content is low, while they may merge to form mesopores with the increasing of nitrogen content.

To further study the functional groups contained in porous carbon samples, we took ANCe-270-1 as an example. The Fourier transform infrared spectroscopy (FT-IR) spectra of the sample ANCe-270-1 is given in Figure 10. Other samples are similar to ANCe-270-1. The peak observed at about 3470 cm^{-1} is the stretching vibration of N−H or −OH, the wider absorption peak at 1630 cm^{-1} is the bending vibration peak of N−H, and the peak at about 1160 cm^{-1} is the stretching absorption peak of C−N. According to the above analysis results, in addition to the hydroxyl group, the porous carbon sample also has other nitrogen-containing functional groups on its surface, indicating the successful doping of nitrogen elements in the carbon structure.

X-ray photoelectron spectroscopy (XPS) is then used to determine the surface chemical properties of carbon materials in

https://doi.org/10.1021/acsomega.1c03664
ACS Omega 2021, 6, 24814−24825

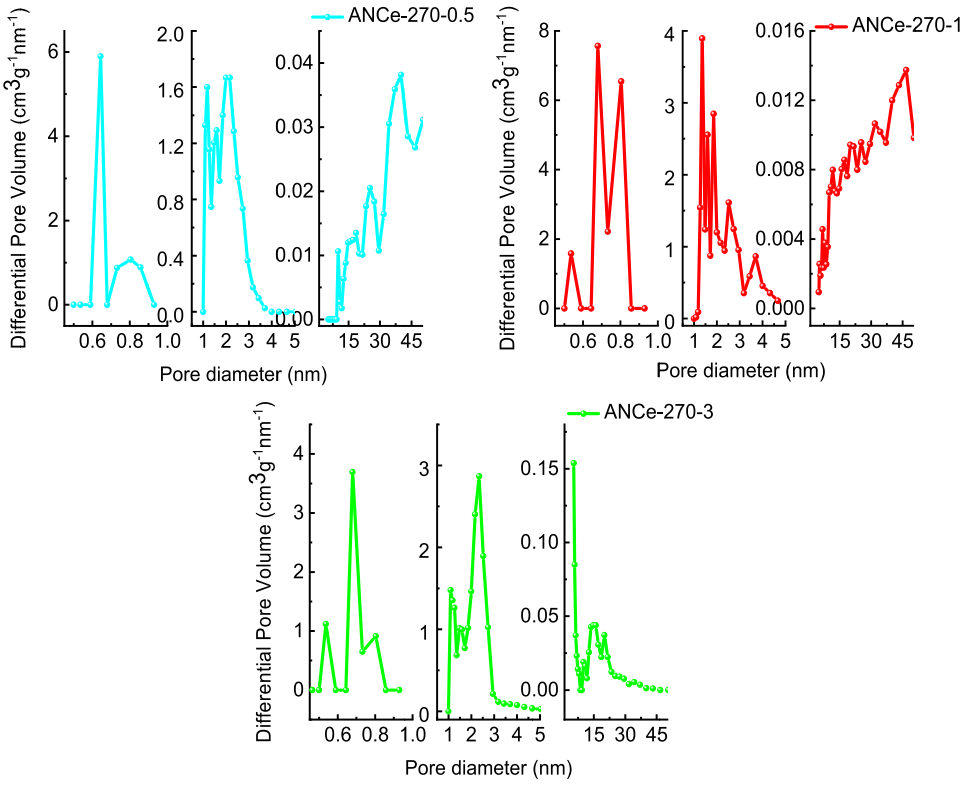

Figure 9. Pore size distribution of different samples.

Table 6. Different Pore Structure Parameters of the Samples

sample	S_{BET} [a] ($m^2 \cdot g^{-1}$)	V_{total} [b] ($cm^3 \cdot g^{-1}$)	S_{micro} [c] ($m^2 \cdot g^{-1}$)	V_{micro} [c] ($cm^3 \cdot g^{-1}$)	D_p [d] (nm)
ANCe-270-3	1437	0.83	1035	0.52	2.38
ANCe-270-1	1703	1.06	1203	0.65	2.21
ANCe-270-0.5	1586	0.91	1154	0.57	2.38

[a]BET surface area. [b]Total pore volume measure at P/P_0 = 0.99. [c]Micropore surface area and micropore volume estimated d < 2 nm by the DFT method. [d]Average pore diameter.

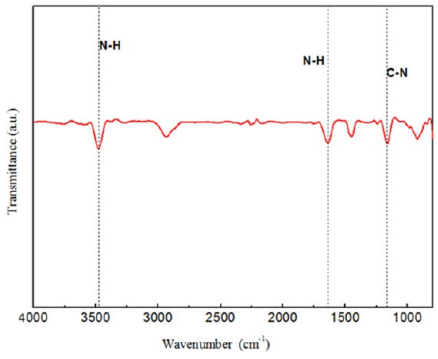

Figure 10. FT-IR spectra of ANCe-270-1.

Figure 11. The wide XPS spectra confirmed three peaks: the pyridina nitrogen peak located near 398 eV, the pyrrole or pyridone nitrogen peak (mainly pyridone nitrogen) located near 400 eV, and a small amount of graphite nitrogen. The C 1s XPS spectra of ANCe-270-1 (60 min) are shown in Figure 12. The C atom mainly exists in the form of C−C (285 eV), C−O (286 eV), and C═O (288 eV). C═O is the characteristic functional group of pyridina. The element analysis is shown in Table 7. The large amounts of nitrogen were detected in all samples, indicating that only a little nitrogen enters the sample interior and most of it is on the sample surface.

2.3. CO_2 Adsorption Study. Table 8 shows the adsorption properties of porous carbon samples with different melamine ratios under different pressures at 25 °C. Compared with the adsorption data of the nitrogen-undoped sample (ACe-270), its adsorption capacity is significantly increased from 0.65 to 1.56 $mmol \cdot g^{-1}$. The reason is that the N-containing groups are beneficial to the chemical adsorption of CO_2. For the same sample, with the increase in pressure, its adsorption capacity gradually increased. Due to the benefit of micropores filling and capillary condensation, the adsorption capacity of CO_2 was improved. Under the same adsorption pressure, with the increase in melamine, the amount of CO_2 adsorption of nitrogen-doped porous carbon samples increases first and then decreases and the orders of their CO_2 adsorption capacities are as follows: ANCe-270-1 > ANCe-270-0.5 > ANCe-270-3. Therefore, ANCe-270-1 has excellent micropore specific surface (1703 $m^2 \cdot g^{-1}$), micropore volume (0.65 $cm^3 \cdot g^{-1}$), and adsorption capacity of CO_2 (7.34 $mmol \cdot g^{-1}$) at 25 °C under the pressure of 0.4 MPa.

2.4. Dynamic Adsorption Study. Figure 13 shows the dynamic adsorption curves and kinetic model curves of the prepared nitrogen-doped porous carbon samples. The kinetic parameters of nitrogen-doped material (ANCe-270-1) and undoped material (ACe-270) at different pressures are shown in Tables 9 and 10. The experimental dynamic adsorption data of the same sample shows that with the increase in pressure, the adsorption line becomes steep and the adsorption equilibrium time becomes longer. This is attributed to the pore structure affects the CO_2 adsorption at different pressures. In the beginning, the adsorption rate of the sample is fast, and the equilibrium adsorption capacity reaches 90% in about 45 min.

https://doi.org/10.1021/acsomega.1c03664
ACS Omega 2021, 6, 24814−24825

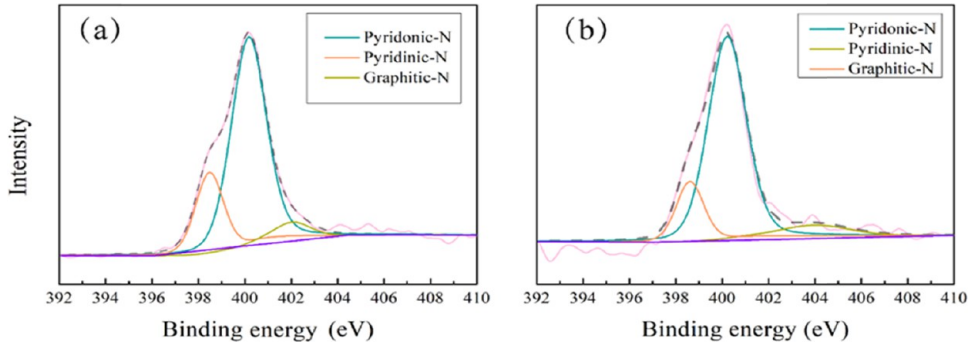

Figure 11. N 1s XPS spectra of ANCe-270-1: (a) 10 min and (b) 60 min.

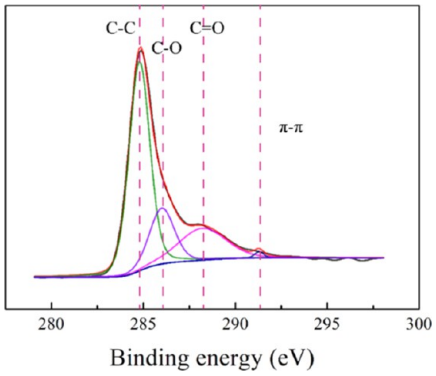

Figure 12. C 1s XPS spectra of ANCe-270-1-60.

Table 7. Relative Atomic Content (atom %) of C 1s, O 1s, and N 1s

	ANCe-270-1-10	ANCe-270-1-60
C 1s	65.85	69.65
O 1s	26.44	22.60
N 1s	7.71	7.75

Table 8. CO_2 Adsorption Properties of the Samples at Different Pressures ($mmol \cdot g^{-1}$)

gas pressure (MPa)	ACe-270	ANCe-270-3	ANCe-270-1	ANCe-270-0.5
0.1	0.65	1.15	1.56	1.41
0.2	1.92	2.81	3.79	3.16
0.3	3.76	4.12	5.42	4.65
0.4	5.23	6.01	7.34	6.59

When the adsorption pressure is low (0.1, 0.2 MPa), the coefficient of determination (R^2) of the pseudo-first-order kinetic model is larger than the pseudo-second-order kinetic model, and the error is smaller. The results show that the kinetic parameters of the pseudo-first-order kinetic model are very close to the experimental data of dynamic adsorption, and the porous carbon materials show mainly physical adsorption. When the adsorption pressure is high (0.3, 0.4 MPa), the R^2 and error of the pseudo-second-order kinetic model are larger and smaller than those of the pseudo-first-order kinetic model, and the kinetic parameters of the pseudo-second-order kinetic model are very close to the experimental dynamic adsorption data, the porous carbon materials mainly show chemical adsorption.[45] By fitting the data, we show that the R^2 and error of the pseudo-first-order kinetic model fitted the undoped materials with the adsorption pressure of 0.3−0.4 MPa and the undoped materials mainly show physical adsorption. While the R^2 and error of the pseudo-second-order kinetic model fitted the doped materials with the adsorption pressure of 0.3−0.4 MPa, and the doped materials mainly show chemical adsorption. It indicates that nitrogen promotes chemical adsorption and improves the CO_2 adsorption of adsorbents. Because the surface of the sample contained nitrogen groups, which promotes the adsorption of CO_2. Other nitrogen-doped samples also conform with this conclusion.[37] Table 11 shows the CO_2 uptake capacities of various sorbents from cellulose at 25 °C and 1 bar. It is significant to study the CO_2 adsorption properties of porous carbon from cellulose.

2.5. Isothermal Adsorption Study. The adsorption data of the prepared porous carbon samples under different pressures and the fitting results of the isothermal model are shown in Figure 14. The Langmuir and Freundlich models are used to analyze the adsorption results. Table 12 shows the relevant parameters of the Langmuir and Freundlich models. By comparing the correlation coefficient (R^2) of different models in Table 12, the coefficients of the Langmuir model and the Freundlich model are similar, but the coefficient of the Freundlich model is closer to 1. The results indicate that the Freundlich model can better simulate and predict the isothermal adsorption performance of nitrogen-doped porous carbon samples. Also, there is chemical adsorption on the surface of the nitrogen-doped porous carbon sample, which is identical to the kinetic simulation results.[50]

3. CONCLUSIONS

In this study, nitrogen-doped porous carbon was successfully prepared from cellulose and melamine by hydrothermal carbonization and KOH chemical activation. A large micropore specific surface area of 1703 $m^2 \cdot g^{-1}$ and high micropore volume of 0.65 $cm^3 \cdot g^{-1}$ could be prepared. Also, a high CO_2 adsorption capacity of 7.34 $mmol \cdot g^{-1}$ at 25 °C under 0.4 MPa pressure could be obtained. The Freundlich isotherm model could describe well the equilibrium data of the prepared samples. When the adsorption pressure is low (0.1, 0.2 MPa), the pseudo-first-order kinetic model is consistent with the experimental dynamic adsorption, and the porous carbon materials mainly show physical adsorption. When the adsorption pressure is high (0.3, 0.4 MPa), the data of the quasi-second-order kinetic model is consistent with the experimental dynamic adsorption. Also, the prepared porous carbon materials are mainly chemical absorption. Overall, nitrogen-doped porous carbon materials have the advantages of low cost and long-term stability for CO_2 capture. Thus, the porous carbon materials are prepared from

https://doi.org/10.1021/acsomega.1c03664
ACS Omega 2021, 6, 24814−24825

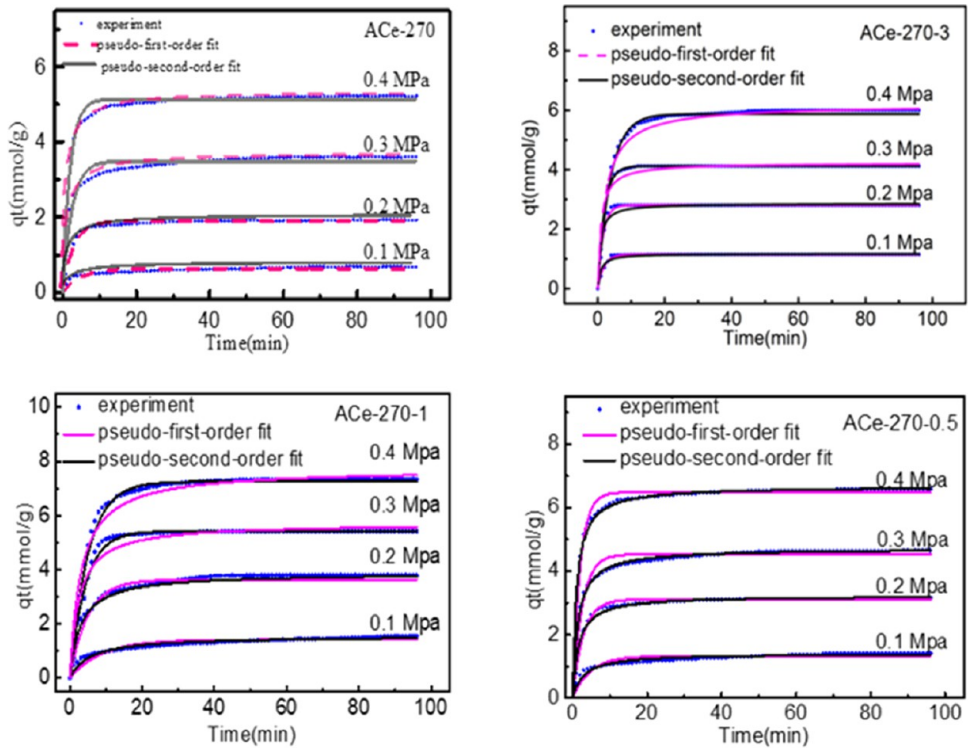

Figure 13. Fitting results of the actual dynamic adsorption process and the kinetic model.

Table 9. Adsorption Kinetic Parameters of ANCe-270-1 at Different Pressures

		pressure (MPa)			
dynamic model	parameter	0.1	0.2	0.3	0.4
pseudo-first-order kinetic	k_1 (min^{-1})	0.2449	0.3821	0.5501	0.4736
	q_e ($mmol·g^{-1}$)	1.55	3.69	5.28	7.12
	R^2	0.9625	0.9701	0.8801	0.8501
	error%	0.95	1.08	8.44	7.59
pseudo-second-order kinetic	k_2 (min^{-1})	0.5863	0.7426	0.5313	0.6612
	q_e ($mmol·g^{-1}$)	1.51	3.62	5.31	7.20
	R^2	0.9432	0.9715	0.9044	0.8903
	error%	0.81	1.06	6.37	5.95

Table 10. Adsorption Kinetic Parameters of ACe-270 at Different Pressures

		pressure (MPa)			
dynamic model	parameter	0.1	0.2	0.3	0.4
pseudo-first-order kinetic	k_1 (min^{-1})	0.6367	0.5737	0.1826	0.4540
	q_e ($mmol·g^{-1}$)	0.64	1.90	3.63	5.17
	R^2	0.9589	0.9496	0.9934	0.9939
	error%	0.07	0.26	0.48	0.32
pseudo-second-order kinetic	k_2 (min^{-1})	2.7827	0.7783	0.0901	0.2226
	q_e ($mmol·g^{-1}$)	0.63	1.88	3.70	5.01
	R^2	0.8013	0.9406	0.9391	0.8716
	error%	0.14	0.35	2.16	1.82

hydrothermal carbonization, chemical activation, and nitrogen doping and have potential use in carbon capture and storage.

Table 11. Properties Comparison of Various Sorbents from Cellulose

materials	S_{BET}[a] ($m^2·g^{-1}$)	V_{micro}[b] ($cm^3·g^{-1}$)	CO_2 uptake (mmol/g)	references
ANCe-270-1	1703	0.65	1.56	present work
Cell-800	2136	0.192	2.54	25
Cell-UK	1147	0.713	5.73	25
CNC	95.2	0.41	2.57	46
K-AC	1978	0.95	5.70	47
LTCA12	806	0.39	2.3	48
AHTC-Cp-270	1634	0.56	0.48	49
AHTC-Ce-270	1482	0.51	0.68	49

[a]BET surface area. [b]micropore volume estimated d < 2 nm by the DFT method.

4. EXPERIMENTAL SECTION

4.1. Synthesis of Porous Carbon. Figure 15 illustrates the preparation process of nitrogen-doped cellulose porous carbons. First, 3 g of microcrystalline cellulose and a certain proportion of melamine were put into a reaction kettle with 100 mL volume, and then 60 mL of deionized water was added into the kettle. The kettle reaction was heated to a certain temperature for the hydrothermal carbonation for 5 h at a heating rate of 5 °C·min^{-1} and then cooled naturally. Subsequently, the solid−liquid mixture of the reaction kettle was washed with deionized water into the filter device and dried at 110 °C to obtain the hydrothermal products. Second, the KOH solid and the hydrothermal products were mixed in a mass ratio of 3:1. The mixture was stirred for 12 h with a magnetic stirrer and then placed in an alumina crucible and heated to 800 °C at 3 °C·min^{-1} under a N_2 atmosphere and held at the temperature for 1 h. The KOH residue was removed by excessive HCl solution and

https://doi.org/10.1021/acsomega.1c03664
ACS Omega 2021, 6, 24814−24825

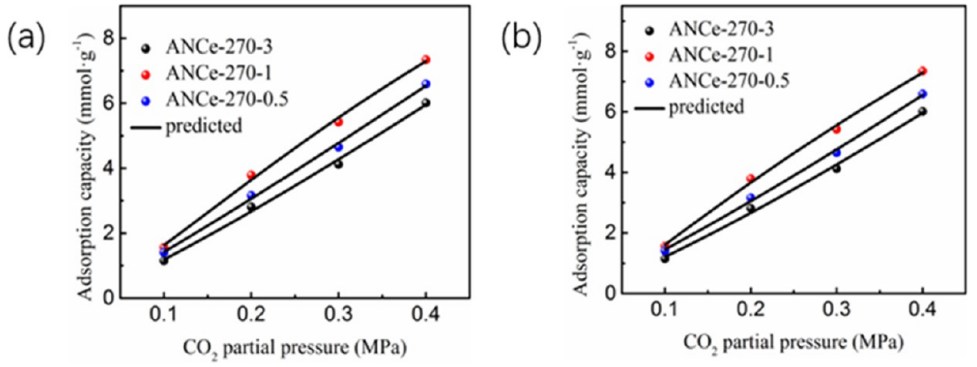

Figure 14. CO_2 adsorption data and adsorption isotherm model: (a) Langmuir model and (b) Freundlich model.

Table 12. Parameters of the Langmuir Model and the Freundlich Model

	Langmuir			Freundlich		
sample	q_m (mmol·g^{-1})	K_L	R^2	K_F	n	R^2
ANCe-270-3	6.59	0.05	0.9887	8.34	0.83	0.9890
ANCe-270-1	23.60	1.41	0.9917	15.23	1.41	0.9932
ANCe-270-0.5	8.62	0.05	0.9941	11.72	0.86	0.9944

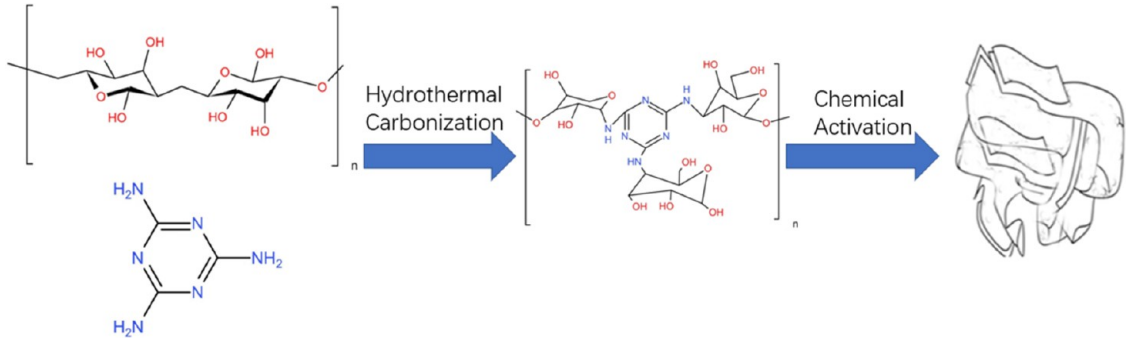

Figure 15. Nitrogen-doped cellulose-based porous carbon reaction process.

then stirred for 12 h. The products were washed repeatedly with deionized water to neutralize the solution. Finally, the filtered solids were dried at 110 °C for 12 h. The hydrothermal products were represented by NCe-*X*-*Y* and the porous carbonized material was denoted by ANCe-*X*-*Y*, *X* was the hydrothermal carbonization temperature of 240, 270, and 300 °C, respectively, and *Y* was the mass ratio of cellulose to melamine of 3, 1, and 0.5, respectively.

4.2. Characterization. The morphology and structure were investigated by FEI/Philips XL30 ESEM FEG field emission scanning electron microscopy (SEM), transmission electron microscopy (TEM), and energy-dispersive spectrometer (EDS). The surface area and pore volume were determined with an N_2 adsorption−desorption isotherm measured at 77 K using a physisorption analyzer (Micromeritics, Model ASAP 2020) determined by the Brunauer−Emmett−Teller (BET) method and the *t*-plot method. The pore size distribution and pore volume were derived from the adsorption branch of isotherm using the density functional theory (DFT) model and the average pore diameter has been calculated by the Barrett−Joyner−Halenda (BJH) method.

4.3. CO_2 Adsorption. The experimental instrument used for CO_2 adsorption/desorption experiments mainly consists of valves, a gas mixing section, an adsorption column, and an online gas chromatograph. Please refer to the literature for the specific calculation and process of CO_2 adsorption.[51]

AUTHOR INFORMATION

Corresponding Author

Guangzhi Yang − *School of Materials Science and Engineering, University of Shanghai for Science and Technology, Shanghai 200093, China;* orcid.org/0000-0003-1811-2214; Phone: +86-21-55270632; Email: yanggzh@usst.edu.cn

Authors

Yifan Tan − *School of Materials Science and Engineering, University of Shanghai for Science and Technology, Shanghai 200093, China*

Xiaoqiang Wang − *School of Materials Science and Engineering, University of Shanghai for Science and Technology, Shanghai 200093, China*

Shen Song − *School of Materials Science and Engineering, University of Shanghai for Science and Technology, Shanghai 200093, China*

Meijiao Sun − *School of Materials Science and Engineering, University of Shanghai for Science and Technology, Shanghai 200093, China*

Yuhua Xue − *School of Materials Science and Engineering, University of Shanghai for Science and Technology, Shanghai 200093, China;* orcid.org/0000-0002-6117-1132

https://doi.org/10.1021/acsomega.1c03664
ACS Omega 2021, 6, 24814−24825

Complete contact information is available at:
https://pubs.acs.org/10.1021/acsomega.1c03664

Notes

The authors declare no competing financial interest.

■ ACKNOWLEDGMENTS

This work is financially supported by the National Natural Science Foundation of China (21875141 and U1760119), the Science and Technology Commission of Shanghai Municipality (19DZ2271100), the Shanghai Scientific and Technological Innovation Project (19JC1410400), and the Innovation Program of Shanghai Municipal Education Commission (2019-01-07-00-07-E00015).

■ REFERENCES

(1) Rahman, F. A.; Aziz, M. M. A.; Saidur, R.; Abu Bakar, W. A. W.; Hainin, M. R.; Putrajaya, R.; Hassan, N. A. Pollution to solution: Capture and sequestration of carbon dioxide (CO_2) and its utilization as a renewable energy source for a sustainable future. *Renewable Sustainble Energy Rev.* **2017**, *71*, 112−126.
(2) Karnauskas, K. B.; Miller, S. L.; Schapiro, A. C. Fossil Fuel Combustion Is Driving Indoor CO_2 Toward Levels Harmful to Human Cognition. *GeoHealth* **2020**, *4*, No. 8.
(3) Zhang, Y.-f.; Yu, C.; Tan, X.-y.; Cui, S.; Li, W.-b.; Qiu, J.-s. Recent advances in multilevel nickel-nitrogen-carbon catalysts for CO_2 electroreduction to CO. *New Carbon Mater.* **2021**, *36*, 19−30.
(4) Anderson, S.; Newell, R. Prospects for carbon capture and storage technologies. *Annu. Rev. Environ. Resour.* **2004**, *29*, 109−142.
(5) Wang, W. J.; Zhouab, M.; Yuan, D. Q. Carbon dioxide capture in amorphous porous organic polymers. *J. Mater. Chem. A* **2017**, *5*, 1334−1347.
(6) Smith, K. H.; Harkin, T.; Mumford, K.; Kentish, S.; Qader, A.; Anderson, C.; Hooper, B.; Stevens, G. W. Outcomes from pilot plant trials of precipitating potassium carbonate solvent absorption for CO_2 capture from a brown coal fired power station in Australia. *Fuel Process. Technol.* **2017**, *155*, 252−260.
(7) Knapik, E.; Kosowski, P.; Stopa, J. Cryogenic liquefaction and separation of CO_2 using nitrogen removal unit cold energy. *Chem. Eng. Res. Des.* **2018**, *131*, 66−79.
(8) Yan, X. R.; Anguille, S.; Bendahan, M.; Moulin, P. Ionic liquids combined with membrane separation processes: A review. *Sep. Purif. Technol.* **2019**, *222*, 230−253.
(9) Chindaprasirt, P.; Rattanasak, U. Characterization of porous alkali-activated fly ash composite as a solid absorbent. *Int. J. Greenhouse Gas Control* **2019**, *85*, 30−35.
(10) Jia, W.; Liu, T.; Li, Q.; Yang, J. Highly efficient photocatalytic reduction of CO_2 on surface-modified Ti-MCM-41 zeolite. *Catal. Today* **2019**, *335*, 221−227.
(11) Wang, W.; Motuzas, J.; Zhao, X. S.; da Costa, J. C. D. Improved CO_2 Sorption in Freeze-Dried Amine Functionalized Mesoporous Silica Sorbent. *Ind. Eng. Chem. Res.* **2018**, *57*, 5653−5660.
(12) Younas, M.; Rezakazemi, M.; Daud, M.; Wazir, M. B.; Ahmad, S.; Ullah, N.; Inamuddin; Ramakrishna, S. Recent progress and remaining challenges in post-combustion CO_2 capture using metal-organic frameworks (MOFs). *Prog. Energy Combust. Sci.* **2020**, *80*, No. 100849.
(13) Rehman, A.; Heo, Y. J.; Nazir, G.; Park, S. J. Solvent-free, one-pot synthesis of nitrogen-tailored alkali-activated microporous carbons with an efficient CO_2 adsorption. *Carbon* **2021**, *172*, 71−82.
(14) Xu, C.; Stromme, M. Sustainable Porous Carbon Materials Derived from Wood-Based Biopolymers for CO_2 Capture. *Nanomaterials* **2019**, *9*, No. 103.
(15) Zhao, Z. J.; Xing, X.; Tang, Z. G.; Zheng, Y.; Fei, W. Y.; Liang, X. F.; Ataeivarjovi, E.; Guo, D. Experiment and simulation study of CO_2 solubility in dimethyl carbonate, 1-octy1-3-methylimidazolium tetrafluoroborate and their mixtures. *Energy* **2018**, *143*, 35−42.
(16) Ren, X. M.; Li, H.; Chen, J.; Wei, L. J.; Modak, A.; Yang, H. Q.; Yang, Q. H. N-doped porous carbons with exceptionally high CO_2 selectivity for CO_2 capture. *Carbon* **2017**, *114*, 473−481.
(17) Arami-Niya, A.; Rufford, T. E.; Zhu, Z. H. Activated carbon monoliths with hierarchical pore structure from tar pitch and coal powder for the adsorption of CO_2, CH_4 and N-2. *Carbon* **2016**, *103*, 115−124.
(18) Wahby, A.; Ramos-Fernandez, J. M.; Martinez-Escandell, M.; Sepulveda-Escribano, A.; Silvestre-Albero, J.; Rodriguez-Reinoso, F. High-Surface-Area Carbon Molecular Sieves for Selective CO_2 Adsorption. *ChemSusChem* **2010**, *3*, 974−981.
(19) Cai, W. Y.; Ding, J.; He, Y. T.; Chen, X. R.; Yuan, D. S.; Chen, C.; Cheng, L. Y.; Du, W.; Wan, H.; Guan, G. F. Nitrogen-Doped Microporous Carbon Prepared by One-Step Carbonization: Rational Design of a Polymer Precursor for Efficient CO_2 Capture. *Energy Fuels* **2021**, *35*, 8857−8867.
(20) Nazir, G.; Rehman, A.; Park, S.-J. Role of heteroatoms (nitrogen and sulfur)-dual doped corn-starch based porous carbons for selective CO_2 adsorption and separation. *J. CO_2 Util.* **2021**, *51*, No. 101641.
(21) Mao, H.; Zhou, D.; Hashisho, Z.; Wang, S.; Chen, H.; Wang, H.; Lashaki, M. J. Microporous activated carbon from pinewood and wheat straw by microwave-assisted KOH treatment for the adsorption of toluene and acetone vapors. *RSC Adv.* **2015**, *5*, 36051−36058.
(22) Malwade, K.; Lataye, D.; Mhaisalkar, V.; Kurwadkar, S.; Ramirez, D. Adsorption of hexavalent chromium onto activated carbon derived from *Leucaena leucocephala* waste sawdust: kinetics, equilibrium and thermodynamics. *Int. J. Environ. Sci. Technol.* **2016**, *13*, 2107−2116.
(23) Islam, M. A.; Tan, I.A.W.; Benhouria, A.; Asif, M.; Hameed, B. H. Mesoporous and adsorptive properties of palm date seed activated carbon prepared via sequential hydrothermal carbonization and sodium hydroxide activation. *Chem. Eng. J.* **2015**, *270*, 187−195.
(24) Li, Y.; Li, Y.; Li, L.; Shi, X.; Wang, Z. Preparation and analysis of activated carbon from sewage sludge and corn stalk. *Adv. Powder Technol.* **2016**, *27*, 684−691.
(25) Rehman, A.; Nazir, G.; Rhee, K. Y.; Park, S. J. A rational design of cellulose-based heteroatom-doped porous carbons: Promising contenders for CO_2 adsorption and separation. *Chem. Eng. J.* **2021**, *420*, No. 130421.
(26) Shi, J.; Cui, H.; Xu, J.; Yan, N.; Zhang, C.; You, S. Fabrication of nitrogen doped and hierarchically porous carbon flowers for CO_2 adsorption. *J. CO_2 Util.* **2021**, *57*, No. 101617.
(27) Lu, Y.; Wang, H.; Yu, P.; Yuan, Y.; Shahbazian-Yassar, R.; Sheng, Y.; Wu, S.; Tu, W.; Liu, G.; Kraft, M.; et al. Isolated Ni single atoms in nitrogen doped ultrathin porous carbon templated from porous g-C_3N_4 for high-performance CO_2 reduction. *Nano Energy* **2020**, *77*, No. 105158.
(28) Li, K.; Liu, S.; Shu, T.; Yan, L.; Guo, H.; Dai, Y.; Luo, X.; Luo, S. Fabrication of carbon microspheres with controllable porous structure by using waste Camellia oleifera shells. *Mater. Chem. Phys.* **2016**, *181*, 518−528.
(29) Li, J.; Michalkiewicz, B.; Min, J.; Ma, C.; Chen, X.; Gong, J.; Mijowska, E.; Tang, T. Selective preparation of biomass-derived porous carbon with controllable pore sizes toward highly efficient CO_2 capture. *Chem. Eng. J.* **2019**, *360*, 250−259.
(30) Chen, W.; Wang, X.; Hashisho, Z.; Feizbakhshan, M.; Shariaty, P.; Niknaddaf, S.; Zhou, X. Template-free and fast one-step synthesis from enzymatic hydrolysis lignin to hierarchical porous carbon for CO_2 capture. *Microporous Mesoporous Mater.* **2019**, *280*, 57−65.
(31) Ma, X.; Li, L.; Chen, R.; Wang, C.; Li, H.; Li, H. Highly Nitrogen-Doped Porous Carbon Derived from Zeolitic Imidazolate Framework-8 for CO_2 Capture. *Chem. − Asian J.* **2018**, *13*, 2069−2076.
(32) Parshetti, G. K.; Chowdhury, S.; Balasubramanian, R. Biomass derived low-cost microporous adsorbents for efficient CO_2 capture. *Fuel* **2015**, *148*, 246−254.
(33) Zhang, C. M.; Song, W.; Ma, Q. L.; Xie, L. J.; Zhang, X. C.; Guo, H. Enhancement of CO_2 Capture on Biomass-Based Carbon from Black Locust by KOH Activation and Ammonia Modification. *Energy Fuels* **2016**, *30*, 4181−4190.

(34) Zhao, Z. N.; Ma, C. D.; Chen, F. Y.; Xu, G. Z.; Pang, R. X.; Qian, X. Y.; Shao, J. W.; Hu, X. Water caltrop shell-derived nitrogen-doped porous carbons with high CO_2 adsorption capacity. *Biomass Bioenergy* **2021**, *145*, No. 105969.
(35) Wei, H. M.; Chen, H. J.; Fu, N.; Chen, J.; Lan, G. X.; Qian, W.; Liu, Y. P.; Lin, H. L.; Han, S. Excellent electrochemical properties and large CO_2 capture of nitrogen-doped activated porous carbon synthesised from waste longan shells. *Electrochim. Acta* **2017**, *231*, 403−411.
(36) Shafeeyan, M. S.; Daud, W.; Houshmand, A.; Arami-Niya, A. Ammonia modification of activated carbon to enhance carbon dioxide adsorption: Effect of pre-oxidation. *Appl. Surf. Sci.* **2011**, *257*, 3936−3942.
(37) Kongnoo, A.; Intharapat, P.; Worathanakul, P.; Phalakornkule, C. Diethanolamine impregnated palm shell activated carbon for CO_2 adsorption at elevated temperatures. *J. Environ. Chem. Eng.* **2016**, *4*, 73−81.
(38) Li, Q.; Liu, S. F.; Wang, L. L.; Chen, F. Y.; Shao, J. W.; Hu, X. Efficient nitrogen doped porous carbonaceous CO_2 adsorbents based on lotus leaf. *J. Environ. Sci.* **2021**, *103*, 268−278.
(39) Liu, S. F.; Rao, L. L.; Yang, P. P.; Wang, X. Y.; Wang, L. L.; Ma, R.; Yue, L. M.; Hu, X. Superior CO_2 uptake on nitrogen doped carbonaceous adsorbents from commercial phenolic resin. *J. Environ. Sci.* **2020**, *93*, 109−116.
(40) Pang, R. X.; Lu, T. Y.; Shao, J. W.; Wang, L. L.; Wu, X. Y.; Qian, X. Y.; Hu, X. Highly Efficient Nitrogen-Doped Porous Carbonaceous CO_2 Adsorbents Derived from Biomass. *Energy Fuels* **2021**, *35*, 1620−1628.
(41) Kamran, U.; Park, S. J. Acetic acid-mediated cellulose-based carbons: Influence of activation conditions on textural features and carbon dioxide uptakes. *J. Colloid Interface Sci.* **2021**, *594*, 745−758.
(42) Li, Y.; Xu, R.; Wang, B.; Wei, J.; Wang, L.; Shen, M.; Yang, J. Enhanced N-doped Porous Carbon Derived from KOH-Activated Waste Wool: A Promising Material for Selective Adsorption of CO_2/CH_4 and CH_4/N_2. *Nanomaterials* **2019**, *9*, No. 266.
(43) Jurewicz, K.; Babel, K.; Ziolkowski, A.; Wachowska, H. Ammoxidation of active carbons for improvement of supercapacitor characteristics. *Electrochim. Acta* **2003**, *48*, 1491−1498.
(44) Sevilla, M.; Fuertes, A. B.; Mokaya, R. High density hydrogen storage in superactivated carbons from hydrothermally carbonized renewable organic materials. *Energy Environ. Sci.* **2011**, *4*, 1400−1410.
(45) Raganati, F.; Alfe, M.; Gargiulo, V.; Chirone, R.; Ammendola, P. Kinetic study and breakthrough analysis of the hybrid physical/chemical CO_2 adsorption/desorption behavior of a magnetite-based sorbent. *Chem. Eng. J.* **2019**, *372*, 526−535.
(46) Xu, J.; Jia, P. P.; Wang, X. J.; Xie, Z. Y.; Chen, Z. Y.; Jiang, H. The aminosilane functionalization of cellulose nanocrystal aerogel via vapor-phase reaction and its CO2 adsorption characteristics. *J. Appl. Polym. Sci.* **2021**, *138*, No. 50891.
(47) Ahmadi, R.; Ardjmand, M.; Rashidi, A.; Rafizadeh, M. High performance novel nanoadsorbents derived-natural cellulose fibers for superior CO_2 adsorption and CO_2/CH_4 separation. *Energy Sources, Part A* **2020**, *19*, 1556−7036.
(48) Geng, S. Y.; Wei, J. Y.; Jonasson, S.; Hedlund, J.; Oksman, K. Multifunctional Carbon Aerogels with Hierarchical Anisotropic Structure Derived from Lignin and Cellulose Nanofibers for CO_2 Capture and Energy Storage. *ACS Appl. Mater. Interfaces* **2020**, *12*, 7432−7441.
(49) Yang, G. Z.; Song, S.; Li, J.; Tang, Z. H.; Ye, J. Y.; Yang, J. H. Preparation and CO_2 adsorption properties of porous carbon by hydrothermal carbonization of tree leaves. *J. Mater. Sci. Technol.* **2019**, *35*, 875−884.
(50) Raganati, F.; Alfe, M.; Gargiulo, V.; Chirone, R.; Ammendola, P. Isotherms and thermodynamics of CO_2 adsorption on a novel carbon-magnetite composite sorbent. *Chem. Eng. Res. Des.* **2018**, *134*, 540−552.
(51) Yang, G.; Ye, J.; Yan, Y.; Tang, Z.; Yu, D.; Yang, J. Preparation and CO_2 adsorption properties of porous carbon from camphor leaves by hydrothermal carbonization and sequential potassium hydroxide activation. *RSC Adv.* **2017**, *7*, 4152−4160.

https://doi.org/10.1021/acsomega.1c03664
ACS Omega 2021, 6, 24814−24825